Topological and Stacked Flat Bands in Bilayer Graphene with a Superlattice Potential

Sayed Ali Akbar Ghorashi[1,*] Aaron Dunbrack[1] Ahmed Abouelkomsan[3] Jiacheng Sun[1]
Xu Du[1] and Jennifer Cano[1,2,†]

[1]*Department of Physics and Astronomy, Stony Brook University, Stony Brook, New York 11794, USA*
[2]*Center for Computational Quantum Physics, Flatiron Institute, New York, New York 10010, USA*
[3]*Department of Physics, Stockholm University, AlbaNova University Center, 106 91 Stockholm, Sweden*

We show that bilayer graphene in the presence of a 2D superlattice potential provides a highly tunable setup that can realize a variety of flat band phenomena. We focus on two regimes: (i) topological flat bands with nonzero Chern numbers, C, including bands with higher Chern numbers $|C| > 1$ and (ii) an unprecedented phase consisting of a stack of nearly perfect flat bands with $C = 0$. For realistic values of the potential and superlattice periodicity, this stack can span nearly 100 meV, encompassing nearly all of the low-energy spectrum. We further show that in the topological regime, the topological flat band has a favorable band geometry for realizing a fractional Chern insulator (FCI) and use exact diagonalization to show that the FCI is in fact the ground state at 1/3 filling. Our results provide a realistic guide for future experiments to realize a new platform for flat band phenomena.

Introduction.—Moiré heterostructures have attracted tremendous interest in recent years, exhibiting a wide variety of phases driven by electron correlations, including superconductivity [1–3], Chern insulators [3–7], Mott insulators [8–10], and Wigner crystals [11]. Underlying the emergence of these phenomena are flat bands. While flat bands were theoretically predicted in twisted bilayer graphene (TBLG) over a decade ago [12,13], seminal experiments [1,8] showing correlated insulators and super-conductivity in magic-angle TBLG ignited a search for flat bands in a variety of systems. In quick succession, new twisted graphene heterostructures entered the scene, such as twisted trilayer and double bilayer graphene [14–22]. Twisted heterostructures beyond graphene include transition metal dichalcogenides [9–11,23–33], magnets [34–36], nodal superconductors [37–39], and topological surface states [40–43].

However, while twisted heterostructures realize a variety of correlated phases on demand, they are not a panacea. Twist angle introduces disorder in the form of inhomog-enous angle and strain. Devices are further complicated by domain formation, lattice relaxation, and the impact of the substrate. Combined, these factors severely hinder sample reproducibility [44].

Thus, it is desirable to explore alternative platforms to realize flat bands and moiré physics. From an electronic structure perspective, the main effect of a twisted moiré heterostructure is to introduce both interlayer tunneling and interlayer potentials on the moiré length scale. The latter can be reproduced by imposing a spatially modulated electric field, which has already been realized on monolayer graphene by inserting a patterned dielectric superlattice

between the gate and the sample, with a periodicity as small as 35 nm [45]. Such a gate-defined superlattice potential also offers control over the superlattice symmetry and geometry.

We introduce Bernal stacked bilayer graphene (BLG) in the presence of a superlattice (SL) potential as a tunable and realistic platform to realize topological flat bands. We envision the experimental setup depicted in Fig. 1(a), where BLG is subject to a spatially varying gate that creates the superlattice, denoted the SL gate, in addition to spatially constant top and bottom gates. We find two distinct regimes of flat bands with possible sub-meV bandwidth, shown schematically in Fig. 1(b), with their corresponding band structures in Figs. 1(c) and 1(d). In the first regime, the flat bands possess a nontrivial (valley) Chern number, $C \neq 0$. Importantly, the flat Chern bands have a near-ideal band geometry [46–48] and realize a fractional Chern insulator (FCI) at 1/3 filling, as we will demonstrate below. Moreover, unlike TBG, our system also realizes sought-after bands with a higher Chern number, $|C| > 1$, which could give rise to exotic FCIs without Landau level analogues [49–58].

The second regime describes a stack of perfect flat bands with $C = 0$, but nonzero Berry curvature. This regime does not require fine-tuning, a situation unprec-edented in TBLG. Remarkably, for a reasonably strong superlattice potential, this stack can span ∼100 meV, covering most of the relevant energy spectrum. In both regimes, we study the role of the superlattice potential period, geometry, and relative potential on each layer, providing a practical guide for experimental realization of *in situ* gate-tunable flat band phenomena.
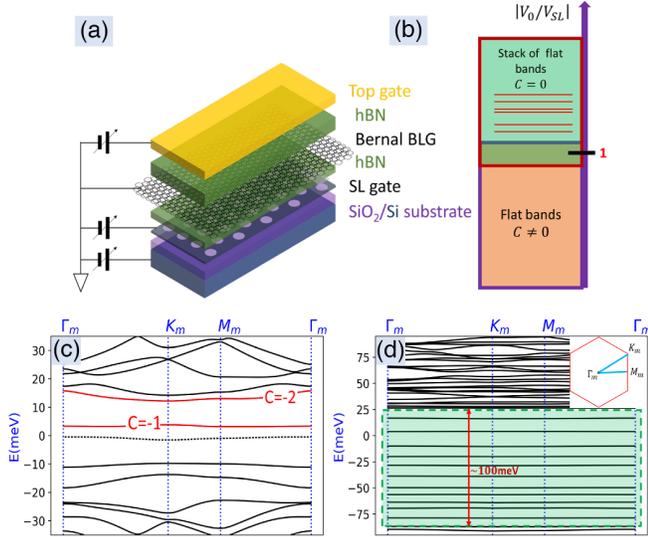
FIG. 1. (a) The proposed experimental setup allows for a tunable displacement field, V_0, and spatially varying superlattice potential, $V_{\rm SL}$. (b) Schematic phase diagram showing stacked and topological flat bands. (c) Energy spectrum of Eq. (1) in the weak field limit, exhibiting a flat Chern band (red, $C = -1$) for representative parameters $V_{\rm SL} = 10, V_0 = -5$ meV. A higher Chern band also appears (red, $C = -2$). Dotted lines indicate the low-energy bands of BLG in the limit $V_{\rm SL} = 0$. (d) The strong field limit exhibits a stack of flat bands (shaded green area) for representative parameters $V_{\rm SL} = 50, V_0 = -70$ meV; mBZ in inset.

Model.—We model biased Bernal BLG in the presence of a superlattice potential by the Hamiltonian

$$\hat{H} = \hat{H}_{\rm BLG} + \hat{H}_{V_0} + \hat{H}_{\rm SL}, \qquad (1)$$

where the three terms describe the Hamiltonian of bilayer graphene, an applied displacement field, and a spatially varying superlattice potential, respectively. Each term is of the form $\hat{H}_i = \int d^2\mathbf{r} H_i(\mathbf{r})\hat{\Psi}^\dagger(\mathbf{r})\hat{\Psi}(\mathbf{r})$, where $\hat{\Psi}(\mathbf{r})$ is the electron annihilation operator at position $\mathbf{r}$, which has implicit layer, sublattice, and valley indices. We now describe each term in detail:

$$H_{\rm BLG}(\mathbf{r}) = \hbar v \tau^0 (-i\chi\partial_x \sigma^1 - i\partial_y\sigma^2) + \frac{t}{2}(\tau^1\sigma^1 - \tau^2\sigma^2) \quad (2)$$

describes biased Bernal BLG, with $\chi = \pm$ the valley index and t the interlayer coupling; Pauli matrices τ and σ correspond to the layer and sublattice spaces. A displacement field V_0 is included via

$$H_{V_0}(\mathbf{r}) = V_0\tau^3\sigma^0. \qquad (3)$$

Finally, the spatially modulated superlattice potential is described by

$$H_{\rm SL}(\mathbf{r}) = \frac{V_{\rm SL}}{2}[(\tau^0 + \tau^3) + \alpha(\tau^0 - \tau^3)]\sigma^0 \sum_n \cos(\mathbf{Q}_n \cdot \mathbf{r}), \qquad (4)$$

where $V_{\rm SL}$ is the strength of the superlattice potential and the set of $\mathbf{Q}_n$ are its wave vectors. We specialize to the case of a triangular superlattice potential with $\mathbf{Q}_n = Q[\cos(2n\pi/6), \sin(2n\pi/6)]$, $n = 1, \ldots, 6$, which define the "mini Brillion zone" (mBZ) by $\Gamma_m = (0, 0)$, $M_m = \frac{1}{2}\mathbf{Q}_0$, and $K_m = (1/3)(\mathbf{Q}_0 + \mathbf{Q}_1)$, as shown in the inset to Fig. 1(d). Note that Γ_m corresponds to the original K point of BLG. The parameter α is the ratio of the superlattice potential felt on one layer relative to the other; the asymmetry between the layers results from the experimental setup [see Fig. 1(a)] where the superlattice gate is applied to only one side of BLG. To be concrete and realistic, in the calculations that follow we take the periodicity of the superlattice to be $L = 50$ nm and the ratio of the potential in each layer to be $\alpha = 0.3$ [59]. We discuss the effects and physical implications of varying L and α at the end of the Letter and in the Supplemental Material [60].

In the proposed setup shown in Fig. 1(a), $V_{\rm SL}$, V_0 and the overall electron density can be tuned independently through the three gates. Thus, there is a vast phase space in which to explore both regimes depicted in Fig. 1(b).

Flat Chern bands in the weak field limit.—In the absence of a superlattice potential ($V_{\rm SL} = 0$), the gate bias V_0 opens a gap at the Dirac points (labeled by Γ_m in the mBZ), which flattens the dispersion at the mBZ center. This gap has been well studied experimentally [61] and theoretically [62–65]. Since the gap has opposite signs in the two valleys, the result is a valley Chern insulator, which exhibits the valley Hall effect [66–71].

Starting from the valley Chern insulator, the role of the superlattice potential $V_{\rm SL}$ is to open gaps at the boundaries of the mBZ, creating an isolated Chern band whose bandwidth is given approximately by the difference between the energy at the mBZ boundary and the gaps opened by V_0 and $V_{\rm SL}$. Since the size of the mBZ scales like $1/L$, appropriate choices of L, V_0, and $V_{\rm SL}$ will yield a nearly flat Chern band gapped from the rest of the spectrum.

We verify this argument by a numerical calculation of the spectrum of Eq. (1) for a superlattice strength $V_{\rm SL} = 10$ meV and displacement potential $V_0 = -5$ meV. The result is shown in Fig. 1(c): the lowest energy conduction band possesses $C = -1$ and has a very small bandwidth, only 0.66 meV. The indirect gaps above and below the flat band are 8.3 and 3.6 meV, respectively. Our calculation also reveals an unexpected feature in the band structure: the next band above the gap is also topological, with a higher Chern number $C = -2$, although it is less flat. Flat bands with higher Chern number $|C| > 1$ are intriguing and sought after because they have no analogue in Landau levels and can realize exotic phases at fractional filling [49–58]. We emphasize that while the flatness is achieved by optimizing the superlattice potential strength, the appearance of Chern bands does not require fine-tuning.

The triangular superlattice potential, unlike the square geometry, induces a particle-hole asymmetry in the
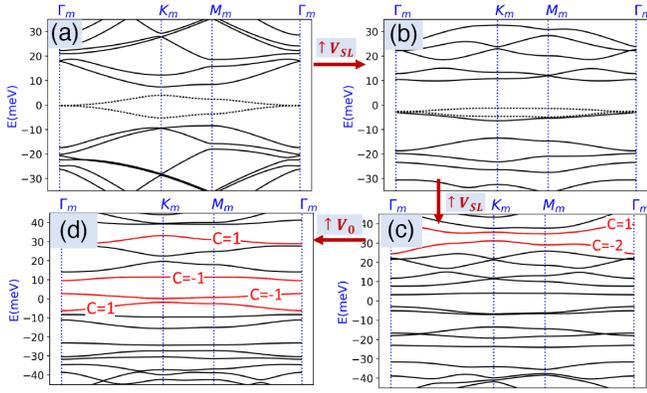
FIG. 2. Band evolution of (1) upon turning up V_{SL}. (a) At zero displacement field ($V_{SL} = 5$, $V_0 = 0$ meV), the combined Chern number of the dotted bands is $C = -1$. Turning up V_{SL} first yields (b) a triple degenerate point ($V_{SL} = 16$, $V_0 = 0$ meV) and then a trivial gap, shown in (c) for $V_{SL} = 20$, $V_0 = 0$ meV. (d) Turning on V_0 from (c) opens topological gaps ($V_{SL} = 20$, $V_0 = 24$ meV). Red lines show topological bands with Chern numbers indicated.

spectrum, as is evident from Figs. 1(c) and 1(d). However, for a weak superlattice potential V_{SL}, the two lowest energy bands [dotted band and red band in Fig. 1(c)] enjoy an approximate particle-hole symmetry. As V_0 and V_{SL} are turned up, multiple band inversions result in a vast and complex space of band structures. In the following, we explore this phase space to determine the effect of the superlattice potential on the bandwidth and topology of BLG.

Flat band engineering with a superlattice potential.— Instead of starting from the valley Chern insulator described above, we now consider $V_0 = 0$ and slowly turn on V_{SL} (Fig. 2). V_{SL} opens gaps at the mBZ boundary, resulting in two low-energy bands (dotted lines), which correspond to the low-energy bands of BLG in the absence of V_{SL}, that detach from the rest of the bands but remain gapless at Γ_m in the absence of V_0. These two bands have a combined Chern number $C = -1$: consistent with our previous argument, turning on small V_0 will open the gap at Γ_m and split them into a trivial and a Chern band [Fig. 1(c)]. Keeping $V_0 = 0$ and continuing to turn up V_{SL}, the two low-energy bands remain gapless up to a critical value of $V_{SL} = 16$ meV where they merge with a third band to form a triple degeneracy at Γ_m, shown in Fig. 2(b). Further increasing V_{SL}, a small gap opens at Γ_m between the two original bands. Though none of the low-energy bands possess $C \neq 0$ [see Fig. 2(c)], relatively flat topological bands emerge at higher energies. Surprisingly, higher Chern number bands appear again, e.g., $C = -2$ in Fig. 2(c). Turning up V_0 from Fig. 2(c) yields several Chern bands with $|C| = 1$, both at the Fermi level and at higher energies, as shown in Fig. 2(d). Summarizing, a triangular superlattice potential, V_{SL}, not only opens a gap at the mBZ boundary but also can induce flat topological

bands, including those with Chern numbers $|C| > 1$. This can occur even in the absence of the displacement field, V_0.

Stack of flat bands.— As topological gaps open away from the original low energy bands of BLG, leading to Chern bands at higher energies, turning up V_0 causes multiple phase transitions and induces a larger gap between the conduction and valence bands. Ultimately, a new regime appears, exhibiting a *stack of flatbands*, indicated by the shaded green region in Fig. 1(d). While these almost perfectly flat bands have vanishing Chern number ($C = 0$), they have nonvanishing Berry curvature. Thus, the electrons are not completely localized in real space. Furthermore, the small bandwidth of the flat bands makes them highly susceptible to the Coulomb interaction, creating a quantum simulator for correlation-driven physics, similar to flat bands in moiré heterostructures [72] but with complete tunability over symmetry and geometry via to the superlattice gate.

The flat band regime can be realized for both signs of V_0, although the spectrum is asymmetric under $V_0 \rightarrow -V_0$ from the asymmetry of the experimental setup [Fig. 1(a)] where the superlattice potential is applied to only one side of the heterostructure. The asymmetry enters Eq. (1) by setting $|\alpha| \neq 1$. Empirically, when V_0 and V_{SL} have opposite signs, a weaker V_0 is required to realize the stack of flat bands (see Ref. [60] for details).

At stronger fields, and keeping $V_0 > V_{SL}$, the stack of flat bands becomes dramatically wider. This is illustrated in Fig. 1(d) with $V_{SL} = 50$, $V_0 = -70$ meV. The stack of flat bands span nearly ~ 100 meV, without fine-tuning V_0 or V_{SL}. A phase with flat bands spanning a wide energy range has not been observed in moiré materials and is in sharp contrast to TBLG, which requires the twist angle be tuned very near the magic angle to realize a single set of isolated flat bands near charge neutrality.

Role of superlattice period and harmonics.— The superlattice period L provides another experimentally accessible tuning knob. While Fig. 2 was computed with $L = 50$ nm, the same phenomena appear for any value of L [60]. Optimizing the value of L in an experiment must balance two considerations: (i) larger L leads to flatter bands at smaller applied fields, making it easier to achieve correlation-driven physics; versus (ii) large L corresponds to a large supercell more susceptible to disorder. Further considerations depend on the precise platform.

Role of α.— The charge distribution of multilayer graphene in a superlattice potential is a complicated problem due to electron screening. We chose $\alpha = 0.3$ following Ref. [59]. To ensure our conclusions are not sensitive to this choice, we explored several other values of α. While changing α qualitatively changes the band structure, the main features discussed in this work, i.e., the generation of topological flat bands and the stack of perfect flat bands, remain intact. Band structures for different values of α are shown in [60], including the special limits $\alpha = 1$ and
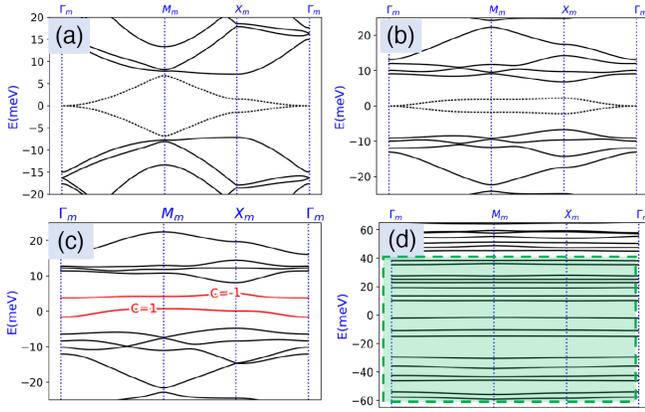
FIG. 3. Band structures for a square superlattice potential. Band structure of Eq. (1) with (a) $V_{SL} = 5, V_0 = 0$ meV; (b) $V_{SL} = 30, V_0 = 0$ meV; (c) $V_{SL} = 30, V_0 = -5$ meV shows red Chern bands; and (d) $V_{SL} = 45, V_0 = -65$ meV shows the stack of flat bands.

FIG. 4. (a) The Berry curvature of the topological flat band labeled by $C = -1$ in Fig. 1(c) in the first mBZ [inset to Fig. 1(d)]. (b) The many-body spectrum (defined relative to the lowest energy value) obtained from momentum space exact diagonalization including a dual-gated Coulomb potential projected onto the $C = -1$ band in Fig. 1(c) at filling $\nu = 1/3$. The inset shows the geometry of the finite cluster used.

$\alpha = -1$ studied in Refs. [73,74]. These values of α are not achievable by the experimental setup in Fig. 1(a), but could be realized by applying two spatially modulated fields symmetrically to the top and bottom layers of BLG, with same or opposite sign.

Lattice geometry.—To investigate the role of superlattice geometry, we show that a square lattice potential yields the same phases achieved with a triangular lattice [Fig. 1(b)], with qualitative differences. Figures 3(a)–3(c) show that, unlike the triangular geometry, in the absence of a displacement field the spectrum remains particle-hole symmetric and gapless for all V_{SL}. The square lattice is less favorable for realizing isolated topological flat bands in the weak potential limit, but tends to require a relatively weaker displacement field V_0 to realize stacks of flat bands [Fig. 3(d)]. The two geometries and their symmetries are described in detail in [60].

Connection to previous work.—Our study of BLG is the first to show a spatially modulated 2D potential creates topological flat bands. It differs from previous studies of BLG in a superlattice potential [73–75] in three fundamental ways: (i) we consider a 2D superlattice; (ii) we consider all four low-energy bands instead of only the lowest two, which is crucial to model the band structure at energies above the interlayer coupling strength; and (iii) importantly, we consider a realistic experimental platform where the spatially modulated field is imposed on only one side of the heterostructure [see Fig. 1(a)]. Previous studies of a superlattice potential on monolayer graphene [45,76–84] and transition metal dichalcogenides [85,86] did not study topological flat bands.

Fractional Chern insulator.—The competition between FCIs and symmetry-broken phases in topological flat bands is of intense current interest [87–93]. The FCI stability is impacted by both bandwidth and band geometry. We have already demonstrated [Fig. 1(c)] that our

platform realizes topological flat bands with sub-meV bandwidth. We now demonstrate their near-ideal band geometry by computing the BZ averaged trace condition: $\bar{T} = \langle T(k) \rangle_{BZ} = \langle \text{Tr}[g(k)] - |\Omega(k)| \rangle_{BZ}$, where $g(k)$ and $\Omega(k)$ are the quantum metric and Berry curvature [shown in Fig. 4(a)], respectively [46–48]. We find $\bar{T} \sim 2.15$, which is a slight improvement over the estimate $\bar{T} = 4$ in TBG [89].

Thus, the band geometry is favorable for realizing an FCI ground state. To verify this single-particle prediction, we perform an exact diagonalization study of the interacting problem of a long range dual-gated Coulomb potential projected onto the Chern band and neglecting its small dispersion. For small system sizes, we find the ground state to be spin and valley polarized (see Supplemental Material [60]). We then compute the many body spectrum assuming spin and valley polarization for a larger system size, shown in Fig. 4(b). We find clear signatures of a Laughlin-like FCI at fractional filling $\nu = 1/3$, specifically, the threefold many-body ground-state degeneracy on the torus, shown in Fig. 4(b), as well as the expected spectral flow and state counting from entanglement spectroscopy [94–98], shown in the Supplemental Material [60].

Discussion.—We introduced BLG in the presence of a superlattice potential as an alternative and tunable platform to realize moiré physics, where the superlattice symmetry and geometry can be chosen on demand. We proposed a realistic experimental design to realize two regimes of gate-tunable flatbands. The first regime exhibits topological flat bands with $C \neq 0$ and, in some instances, more exotic higher Chern numbers with $|C| > 1$. Of particular interest is a isolated $C = -1$ band with sub-meV bandwidth, whose quantum geometry is favorable for realizing an FCI ground state at fractional filling. This single-particle prediction is verified by exact diagonalization including a screened Coulomb interaction projected into the topological flat band, which reveals a Laughlin-like ground state. A more thorough multi-band calculation will be carried out in future work.

The second regime realizes a stack of many isolated almost perfectly flat bands with $C = 0$. Again the bandwidth is ~ 1 meV. Although these bands are topologically trivial, they have nonvanishing Berry curvature and may also exhibit interesting correlated phases at integer or fractional filling. The possibility of superconducting phases analogous to the observation in TBG [1–3] are of particular interest.

Note added in proof.—Our results motivate the experimental study of BLG with a superlattice potential to achieve topological and nontopological flat bands without fine-tuning twist angle or introducing twist disorder. Recently, we have shown that similar phases may be realized in multilayer graphene in the presence of a superlattice potential [99].

---

[*] sayedaliakbar.ghorashi@stonybrook.edu
[†] jennifer.cano@stonybrook.edu

[1] Y. Cao, V. Fatemi, S. Fang, K. Watanabe, T. Taniguchi, E. Kaxiras, and P. Jarillo-Herrero, Unconventional superconductivity in magic-angle graphene superlattices, Nature (London) **556**, 43 (2018).

[2] M. Yankowitz, S. Chen, H. Polshyn, Y. Zhang, K. Watanabe, T. Taniguchi, D. Graf, A. F. Young, and C. R. Dean, Tuning superconductivity in twisted bilayer graphene, Science **363**, 1059 (2019).

[3] X. Lu, P. Stepanov, W. Yang, M. Xie, M. A. Aamir, I. Das, C. Urgell, K. Watanabe, T. Taniguchi, G. Zhang, A. Bachtold, A. H. MacDonald, and D. K. Efetov, Superconductors, orbital magnets and correlated states in magic-angle bilayer graphene, Nature (London) **574**, 653 (2019).

[4] M. Serlin, C. Tschirhart, H. Polshyn, Y. Zhang, J. Zhu, K. Watanabe, T. Taniguchi, L. Balents, and A. Young, Intrinsic quantized anomalous hall effect in a moiré heterostructure, Science **367**, 900 (2020).

[5] K. P. Nuckolls, M. Oh, D. Wong, B. Lian, K. Watanabe, T. Taniguchi, B. A. Bernevig, and A. Yazdani, Strongly correlated chern insulators in magic-angle twisted bilayer graphene, Nature (London) **588**, 610 (2020).

[6] G. Chen, A. L. Sharpe, E. J. Fox, Y.-H. Zhang, S. Wang, L. Jiang, B. Lyu, H. Li, K. Watanabe, T. Taniguchi, Z. Shi, T. Senthil, D. Goldhaber-Gordon, Y. Zhang, and F. Wang, Tunable correlated Chern insulator and ferromagnetism in a moiré superlattice, Nature (London) **579**, 56 (2020).

[7] Y. Xie, A. T. Pierce, J. M. Park, D. E. Parker, E. Khalaf, P. Ledwith, Y. Cao, S. H. Lee, S. Chen, P. R. Forrester, K. Watanabe, T. Taniguchi, A. Vishwanath, P. Jarillo-Herrero, and A. Yacoby, Fractional chern insulators in magic-angle twisted bilayer graphene, Nature (London) **600**, 439 (2021).

[8] Y. Cao, V. Fatemi, A. Demir, S. Fang, S. L. Tomarken, J. Y. Luo, J. D. Sanchez-Yamagishi, K. Watanabe, T. Taniguchi, E. Kaxiras, R. C. Ashoori, and P. Jarillo-Herrero, Correlated insulator behaviour at half-filling in magic-angle graphene superlattices, Nature (London) **556**, 80 (2018).

[9] Y. Xu, S. Liu, D. A. Rhodes, K. Watanabe, T. Taniguchi, J. Hone, V. Elser, K. F. Mak, and J. Shan, Correlated insulating states at fractional fillings of moiré superlattices, Nature (London) **587**, 214 (2020).

[10] Y. Tang, L. Li, T. Li, Y. Xu, S. Liu, K. Barmak, K. Watanabe, T. Taniguchi, A. H. MacDonald, J. Shan, and K. F. Mak, Simulation of Hubbard model physics in WSe_2/WS_2 moiré superlattices, Nature (London) **579**, 353 (2020).

[11] E. C. Regan, D. Wang, C. Jin, M. I. B. Utama, B. Gao, X. Wei, S. Zhao, W. Zhao, Z. Zhang, K. Yumigeta, M. Blei, J. D. Carlstrm, K. Watanabe, T. Taniguchi, S. Tongay, M. Crommie, A. Zettl, and F. Wang, Mott and generalized Wigner crystal states in WSe_2/WS_2 moiré superlattices, Nature (London) **579**, 359 (2020).

[12] R. Bistritzer and A. H. MacDonald, Moiré bands in twisted double-layer graphene, Proc. Natl. Acad. Sci. U.S.A. **108**, 12233 (2011).

[13] E. Suárez Morell, J. D. Correa, P. Vargas, M. Pacheco, and Z. Barticevic, Flat bands in slightly twisted bilayer graphene: Tight-binding calculations, Phys. Rev. B **82**, 121407(R) (2010).

[14] X. Liu, Z. Hao, E. Khalaf, J. Y. Lee, Y. Ronen, H. Yoo, D. H. Najafabadi, K. Watanabe, T. Taniguchi, A. Vishwanath, and P. Kim, Tunable spin-polarized correlated states in twisted double bilayer graphene, Nature (London) **583**, 221 (2020).

[15] M. He, Y. Li, J. Cai, Y. Liu, K. Watanabe, T. Taniguchi, X. Xu, and M. Yankowitz, Symmetry breaking in twisted double bilayer graphene, Nat. Phys. **17**, 26 (2021).

[16] G. W. Burg, J. Zhu, T. Taniguchi, K. Watanabe, A. H. MacDonald, and E. Tutuc, Correlated Insulating States in Twisted Double Bilayer Graphene, Phys. Rev. Lett. **123**, 197702 (2019).

[17] C. Shen, Y. Chu, Q. Wu, N. Li, S. Wang, Y. Zhao, J. Tang, J. Liu, J. Tian, K. Watanabe, R. Yang, Z. Y. Meng, D. Shi, O. V. Yazyev, and G. Zhang, Correlated states in twisted double bilayer graphene, Nat. Phys. **16**, 520 (2020).

[18] Y. Cao, D. Rodan-Legrain, O. Rubies-Bigorda, J. M. Park, K. Watanabe, T. Taniguchi, and P. Jarillo-Herrero, Tunable correlated states and spin-polarized phases in twisted bilayer-bilayer graphene, Nature (London) **583**, 215 (2020).

[19] J. M. Park, Y. Cao, K. Watanabe, T. Taniguchi, and P. Jarillo-Herrero, Tunable strongly coupled superconductivity in magic-angle twisted trilayer graphene, Nature (London) **590**, 249 (2021).

[20] S. Xu, M. M. A. Ezzi, N. Balakrishnan, A. Garcia-Ruiz, B. Tsim, C. Mullan, J. Barrier, N. Xin, B. A. Piot, T. Taniguchi, K. Watanabe, A. Carvalho, A. Mishchenko, A. K. Geim, V. I. Fal'ko, S. Adam, A. H. C. Neto, K. S. Novoselov, and Y. Shi, Tunable van Hove singularities and correlated states

in twisted monolayer–bilayer graphene, Nat. Phys. **17**, 619 (2021).

[21] S. Chen, M. He, Y.-H. Zhang, V. Hsieh, Z. Fei, K. Watanabe, T. Taniguchi, D. H. Cobden, X. Xu, C. R. Dean, and M. Yankowitz, Electrically tunable correlated and topological states in twisted monolayer-bilayer graphene, Nat. Phys. **17**, 374 (2021).

[22] Z. Hao, A. Zimmerman, P. Ledwith, E. Khalaf, D. H. Najafabadi, K. Watanabe, T. Taniguchi, A. Vishwanath, and P. Kim, Electric field–tunable superconductivity in alternating-twist magic-angle trilayer graphene, Science **371**, 1133 (2021).

[23] F. Wu, T. Lovorn, E. Tutuc, I. Martin, and A. H. MacDonald, Topological Insulators in Twisted Transition Metal Dichalcogenide Homobilayers, Phys. Rev. Lett. **122**, 086402 (2019).

[24] L. Wang, E.-M. Shih, A. Ghiotto, L. Xian, D. A. Rhodes, C. Tan, M. Claassen, D. M. Kennes, Y. Bai, B. Kim, K. Watanabe, T. Taniguchi, X. Zhu, J. Hone, A. Rubio, A. N. Pasupathy, and C. R. Dean, Correlated electronic phases in twisted bilayer transition metal dichalcogenides, Nat. Mater. **19**, 861 (2020).

[25] F. Wu, T. Lovorn, E. Tutuc, and A. H. MacDonald, Hubbard Model Physics in Transition Metal Dichalcogenide Moiré Bands, Phys. Rev. Lett. **121**, 026402 (2018).

[26] T. Devakul, V. Crépel, Y. Zhang, and L. Fu, Magic in twisted transition metal dichalcogenide bilayers, Nat. Commun. **12**, 6730 (2021).

[27] J. Zang, J. Wang, J. Cano, and A. J. Millis, Hartree-Fock study of the moiré Hubbard model for twisted bilayer transition metal dichalcogenides, Phys. Rev. B **104**, 075150 (2021).

[28] Z. Bi and L. Fu, Excitonic density wave and spin-valley superfluid in bilayer transition metal dichalcogenide, Nat. Commun. **12**, 642 (2021).

[29] J. Wang, J. Zang, J. Cano, and A. J. Millis, Staggered pseudo magnetic field in twisted transition metal dichalcogenides: Physical origin and experimental consequences, Phys. Rev. Res. **5**, L012005 (2023).

[30] J. Zang, J. Wang, J. Cano, A. Georges, and A. J. Millis, Dynamical Mean Field Theory of Moiré Bilayer Transition Metal Dichalcogenides: Phase Diagram, Resistivity, and Quantum Criticality, Phys. Rev. X **12**, 021064 (2022).

[31] A. Wietek, J. Wang, J. Zang, J. Cano, A. Georges, and A. Millis, Tunable stripe order and weak superconductivity in the moiré Hubbard model, Phys. Rev. Res. **4**, 043048 (2022).

[32] L. Xian, M. Claassen, D. Kiese, M. M. Scherer, S. Trebst, D. M. Kennes, and A. Rubio, Realization of nearly dispersionless bands with strong orbital anisotropy from destructive interference in twisted bilayer MoS_2, Nat. Commun. **12**, 5644 (2021).

[33] L. Klebl, Q. Xu, A. Fischer, L. Xian, M. Claassen, A. Rubio, and D. M. Kennes, Moiré engineering of spin-orbit coupling in twisted platinum diselenide, Electron. Struct. **4**, 014004 (2022).

[34] K. Hejazi, Z.-X. Luo, and L. Balents, Noncollinear phases in moiré magnets, Proc. Natl. Acad. Sci. U.S.A. **117**, 10721 (2020).

[35] Y. Xu, A. Ray, Y.-T. Shao, S. Jiang, D. Weber, J. E. Goldberger, K. Watanabe, T. Taniguchi, D. A. Muller,

K. F. Mak, and J. Shan, Emergence of a noncollinear magnetic state in twisted bilayer CrI_3, arXiv:2103.09850.

[36] T. Song, Q.-C. Sun, E. Anderson, C. Wang, J. Qian, T. Taniguchi, K. Watanabe, M. A. McGuire, R. Stöhr, D. Xiao, T. Cao, J. Wrachtrup, and X. Xu, Direct visualization of magnetic domains and moiré magnetism in twisted 2d magnets, Science **374**, 1140 (2021).

[37] P. A. Volkov, J. H. Wilson, and J. Pixley, Magic angles and current-induced topology in twisted nodal superconductors, Phys. Rev. B **107**, 174506 (2023).

[38] O. Can, T. Tummuru, R. P. Day, I. Elfimov, A. Damascelli, and M. Franz, High-temperature topological superconductivity in twisted double-layer copper oxides, Nat. Phys. **17**, 519 (2021).

[39] S. Y. F. Zhao, N. Poccia, X. Cui, P. A. Volkov, H. Yoo, R. Engelke, Y. Ronen, R. Zhong, G. Gu, S. Plugge, T. Tummuru, M. Franz, J. H. Pixley, and P. Kim, Emergent interfacial superconductivity between twisted cuprate superconductors, arXiv:2108.13455.

[40] J. Cano, S. Fang, J. H. Pixley, and J. H. Wilson, Moiré superlattice on the surface of a topological insulator, Phys. Rev. B **103**, 155157 (2021).

[41] T. Wang, N. F. Q. Yuan, and L. Fu, Moiré Surface States and Enhanced Superconductivity in Topological Insulators, Phys. Rev. X **11**, 021024 (2021).

[42] A. Dunbrack and J. Cano, Magic angle conditions for twisted 3d topological insulators, Phys. Rev. B **106**, 075142 (2022).

[43] D. Guerci, J. Wang, J. H. Pixley, and J. Cano, Designer meron lattice on the surface of a topological insulator, Phys. Rev. B **106**, 245417 (2022).

[44] C. N. Lau, M. W. Bockrath, K. F. Mak, and F. Zhang, Reproducibility in the fabrication and physics of moiré materials, Nature (London) **602**, 41 (2022).

[45] C. Forsythe, X. Zhou, K. Watanabe, T. Taniguchi, A. Pasupathy, P. Moon, M. Koshino, P. Kim, and C. R. Dean, Band structure engineering of 2d materials using patterned dielectric superlattices, Nat. Nanotechnol. **13**, 566 (2018).

[46] T. S. Jackson, G. Möller, and R. Roy, Geometric stability of topological lattice phases, Nat. Commun. **6**, 8629 (2015).

[47] R. Roy, Band geometry of fractional topological insulators, Phys. Rev. B **90**, 165139 (2014).

[48] S. A. Parameswaran, R. Roy, and S. L. Sondhi, Fractional Chern insulators and the W_{∞} algebra, Phys. Rev. B **85**, 241308(R) (2012).

[49] Z. Liu, E. J. Bergholtz, H. Fan, and A. M. Läuchli, Fractional Chern Insulators in Topological Flat Bands with Higher Chern Number, Phys. Rev. Lett. **109**, 186805 (2012).

[50] S. Yang, Z.-C. Gu, K. Sun, and S. Das Sarma, Topological flat band models with arbitrary Chern numbers, Phys. Rev. B **86**, 241112(R) (2012).

[51] Y.-F. Wang, H. Yao, C.-D. Gong, and D. N. Sheng, Fractional quantum Hall effect in topological flat bands with Chern number two, Phys. Rev. B **86**, 201101(R) (2012).

[52] A. Sterdyniak, C. Repellin, B. A. Bernevig, and N. Regnault, Series of Abelian and non-Abelian states in $c > 1$ fractional Chern insulators, Phys. Rev. B **87**, 205137 (2013).

[53] Y.-L. Wu, N. Regnault, and B. A. Bernevig, Bloch Model Wave Functions and Pseudopotentials for All Fractional Chern Insulators, Phys. Rev. Lett. 110, 106802 (2013).

[54] G. Möller and N. R. Cooper, Fractional Chern Insulators in Harper-Hofstadter Bands with Higher Chern Number, Phys. Rev. Lett. 115, 126401 (2015).

[55] Y.-H. Wu, J. K. Jain, and K. Sun, Fractional topological phases in generalized Hofstadter bands with arbitrary Chern numbers, Phys. Rev. B 91, 041119(R) (2015).

[56] J. Behrmann, Z. Liu, and E. J. Bergholtz, Model Fractional Chern Insulators, Phys. Rev. Lett. 116, 216802 (2016).

[57] B. Andrews and G. Möller, Stability of fractional Chern insulators in the effective continuum limit of Harper-Hofstadter bands with Chern number $|c| > 1$, Phys. Rev. B 97, 035159 (2018).

[58] J. Wang and Z. Liu, Hierarchy of Ideal Flatbands in Chiral Twisted Multilayer Graphene Models, Phys. Rev. Lett. 128, 176403 (2022).

[59] H. Rokni and W. Lu, Layer-by-layer insight into electrostatic charge distribution of few-layer graphene, Sci. Rep. 7, 42821 (2017).

[60] See Supplemental Material at http://link.aps.org/supplemental/10.1103/PhysRevLett.130.196201 for more details.

[61] T. Ohta, A. Bostwick, T. Seyller, K. Horn, and E. Rotenberg, Controlling the electronic structure of bilayer graphene, Science 313, 951 (2006).

[62] E. McCann, Asymmetry gap in the electronic band structure of bilayer graphene, Phys. Rev. B 74, 161403(R) (2006).

[63] E. McCann and V. I. Fal'ko, Landau-Level Degeneracy and Quantum Hall Effect in a Graphite Bilayer, Phys. Rev. Lett. 96, 086805 (2006).

[64] E. V. Castro, K. S. Novoselov, S. V. Morozov, N. M. R. Peres, J. M. B. L. Dos Santos, J. Nilsson, F. Guinea, A. K. Geim, and A. H. Castro Neto, Biased Bilayer Graphene: Semiconductor with a Gap Tunable by the Electric Field Effect, Phys. Rev. Lett. 99, 216802 (2007).

[65] H. Min, B. Sahu, S. K. Banerjee, and A. H. MacDonald, Ab initio theory of gate induced gaps in graphene bilayers, Phys. Rev. B 75, 155115 (2007).

[66] D. Xiao, W. Yao, and Q. Niu, Valley-Contrasting Physics in Graphene: Magnetic Moment and Topological Transport, Phys. Rev. Lett. 99, 236809 (2007).

[67] J. Jung, F. Zhang, Z. Qiao, and A. H. MacDonald, Valley-Hall kink and edge states in multilayer graphene, Phys. Rev. B 84, 075418 (2011).

[68] W. Yao, D. Xiao, and Q. Niu, Valley-dependent optoelectronics from inversion symmetry breaking, Phys. Rev. B 77, 235406 (2008).

[69] D. Xiao, G.-B. Liu, W. Feng, X. Xu, and W. Yao, Coupled Spin and Valley Physics in Monolayers of MoS_2 and Other Group-VI Dichalcogenides, Phys. Rev. Lett. 108, 196802 (2012).

[70] R. V. Gorbachev, J. C. W. Song, G. L. Yu, A. V. Kretinin, F. Withers, Y. Cao, A. Mishchenko, I. V. Grigorieva, K. S. Novoselov, L. S. Levitov, and A. K. Geim, Detecting topological currents in graphene superlattices, Science 346, 448 (2014).

[71] K. F. Mak, K. L. McGill, J. Park, and P. L. McEuen, The valley hall effect in MoS_2 transistors, Science 344, 1489 (2014).

[72] D. M. Kennes, M. Claassen, L. Xian, A. Georges, A. J. Millis, J. Hone, C. R. Dean, D. Basov, A. N. Pasupathy, and A. Rubio, Moiré heterostructures as a condensed-matter quantum simulator, Nat. Phys. 17, 155 (2021).

[73] M. Killi, S. Wu, and A. Paramekanti, Band Structures of Bilayer Graphene Superlattices, Phys. Rev. Lett. 107, 086801 (2011).

[74] S. Wu, M. Killi, and A. Paramekanti, Graphene under spatially varying external potentials: Landau levels, magnetotransport, and topological modes, Phys. Rev. B 85, 195404 (2012).

[75] A. Ramires and J. L. Lado, Electrically Tunable Gauge Fields in Tiny-Angle Twisted Bilayer Graphene, Phys. Rev. Lett. 121, 146801 (2018).

[76] C.-H. Park, L. Yang, Y.-W. Son, M. L. Cohen, and S. G. Louie, Anisotropic behaviours of massless Dirac fermions in graphene under periodic potentials, Nat. Phys. 4, 213 (2008).

[77] C.-H. Park, L. Yang, Y.-W. Son, M. L. Cohen, and S. G. Louie, New Generation of Massless Dirac Fermions in Graphene under External Periodic Potentials, Phys. Rev. Lett. 101, 126804 (2008).

[78] C.-H. Park and S. G. Louie, Making massless Dirac fermions from a patterned two-dimensional electron gas, Nano Lett. 9, 1793 (2009).

[79] M. Barbier, P. Vasilopoulos, and F. M. Peeters, Extra Dirac points in the energy spectrum for superlattices on single-layer graphene, Phys. Rev. B 81, 075438 (2010).

[80] S. Dubey, V. Singh, A. K. Bhat, P. Parikh, S. Grover, R. Sensarma, V. Tripathi, K. Sengupta, and M. M. Deshmukh, Tunable superlattice in graphene to control the number of Dirac points, Nano Lett. 13, 3990 (2013).

[81] L. A. Ponomarenko, R. V. Gorbachev, G. L. Yu, D. C. Elias, R. Jalil, A. A. Patel, A. Mishchenko, A. S. Mayorov, C. R. Woods, J. R. Wallbank, M. Mucha-Kruczynski, B. A. Piot, M. Potemski, I. V. Grigorieva, K. S. Novoselov, F. Guinea, V. I. Fal'ko, and A. K. Geim, Cloning of Dirac fermions in graphene superlattices, Nature (London) 497, 594 (2013).

[82] R. Huber, M.-H. Liu, S.-C. Chen, M. Drienovsky, A. Sandner, K. Watanabe, T. Taniguchi, K. Richter, D. Weiss, and J. Eroms, Gate-tunable two-dimensional super-lattices in graphene, Nano Lett. 20, 8046 (2020).

[83] Y. Li, S. Dietrich, C. Forsythe, T. Taniguchi, K. Watanabe, P. Moon, and C. R. Dean, Anisotropic band flattening in graphene with one-dimensional superlattices, Nat. Nanotechnol. 16, 525 (2021).

[84] X. Lu, S. Zhang, Z. V. Han, and J. Liu, Synergistic interplay between dirac fermions and long-wavelength order parameters in graphene-insulator heterostructures, arXiv:2206.05659.

[85] L.-k. Shi, J. Ma, and J. C. Song, Gate-tunable flat bands in van der Waals patterned dielectric superlattices, 2D Mater. 7, 015028 (2019).

[86] X.-C. Yang, H. Yu, and W. Yao, Chiral Excitonics in Monolayer Semiconductors on Patterned Dielectrics, Phys. Rev. Lett. 128, 217402 (2022).

[87] A. Abouelkomsan, Z. Liu, and E. J. Bergholtz, Particle-Hole Duality, Emergent Fermi Liquids, and Fractional Chern Insulators in Moiré Flatbands, Phys. Rev. Lett. 124, 106803 (2020).

[88] C. Repellin and T. Senthil, Chern bands of twisted bilayer graphene: Fractional Chern insulators and spin phase transition, Phys. Rev. Res. **2,** 023238 (2020).

[89] P. J. Ledwith, G. Tarnopolsky, E. Khalaf, and A. Vishwanath, Fractional Chern insulator states in twisted bilayer graphene: An analytical approach, Phys. Rev. Res. **2,** 023237 (2020).

[90] J. Wang, J. Cano, A. J. Millis, Z. Liu, and B. Yang, Exact Landau Level Description of Geometry and Interaction in a Flatband, Phys. Rev. Lett. **127,** 246403 (2021).

[91] P. Wilhelm, T. C. Lang, and A. M. Läuchli, Interplay of fractional Chern insulator and charge density wave phases in twisted bilayer graphene, Phys. Rev. B **103,** 125406 (2021).

[92] H. Li, U. Kumar, K. Sun, and S.-Z. Lin, Spontaneous fractional Chern insulators in transition metal dichalcogenide moiré superlattices, Phys. Rev. Res. **3,** L032070 (2021).

[93] A. Abouelkomsan, K. Yang, and E. J. Bergholtz, Quantum metric induced phases in moiré materials, Phys. Rev. Res. **5,** L012015 (2023).

[94] H. Li and F. D. M. Haldane, Entanglement Spectrum as a Generalization of Entanglement Entropy: Identification of Topological Order in Non-Abelian Fractional Quantum Hall Effect States, Phys. Rev. Lett. **101,** 010504 (2008).

[95] B. A. Bernevig and N. Regnault, Emergent many-body translational symmetries of Abelian and non-Abelian fractionally filled topological insulators, Phys. Rev. B **85,** 075128 (2012).

[96] A. Sterdyniak, N. Regnault, and B. A. Bernevig, Extracting Excitations from Model State Entanglement, Phys. Rev. Lett. **106,** 100405 (2011).

[97] Y.-L. Wu, N. Regnault, and B. A. Bernevig, Haldane statistics for fractional Chern insulators with an arbitrary Chern number, Phys. Rev. B **89,** 155113 (2014).

[98] N. Regnault, Entanglement spectroscopy and its application to the quantum Hall effects, arXiv:1510.07670.

[99] Sayed Ali Akbar Ghorashi and Jennifer Cano, companion paper, Multilayer graphene with a superlattice potential, Phys. Rev. B **107,** 195423 (2023).